Northumbria Research Link

Northumbria
University
NEWCASTLE

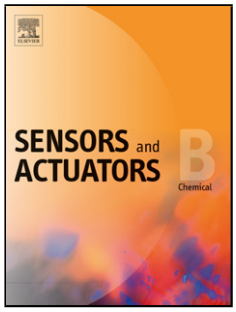

Title: Colloidal quantum dot-based surface acoustic wave sensors for NO_2-sensing behavior

Authors: Min Li, Hao Kan, Shutian Chen, Xiaoying Feng, Hui Li, Chong Li, Chen Fu, Aojie Quan, Huibin Sun, Jingting Luo, Xueli Liu, Wen Wang, Huan Liu, Qiuping Wei, Yongqing Fu

PII: S0925-4005(19)30253-9
DOI: https://doi.org/10.1016/j.snb.2019.02.042
Reference: SNB 26137

To appear in: *Sensors and Actuators B*

Received date: 30 July 2018
Revised date: 18 December 2018
Accepted date: 10 February 2019

Please cite this article as: Li M, Kan H, Chen S, Feng X, Li H, Li C, Fu C, Quan A, Sun H, Luo J, Liu X, Wang W, Liu H, Wei Q, Fu Y, Colloidal quantum dot-based surface acoustic wave sensors for NO_2-sensing behavior, *Sensors and amp; Actuators: B. Chemical* (2019), https://doi.org/10.1016/j.snb.2019.02.042

Colloidal quantum dot-based surface acoustic wave sensors for NO_2-sensing behavior

Min Li[a,b], Hao Kan[a,b], Shutian Chen[c], Xiaoying Feng[a], Hui Li[a], Chong Li[a], Chen Fu[a], Aojie Quan[a], Huibin Sun[a], Jingting Luo[a,*], Xueli Liu[d], Wen Wang[d,*], Huan Liu[e], Qiuping Wei[f], Yongqing Fu[g]

[a] Shenzhen Key Laboratory of Advanced Thin Films and Applications, College of Physics and Energy, Shenzhen University, 518060, Shenzhen, China

[b] Key Laboratory of Optoelectronic Devices and Systems of Ministry of Education and Guangdong Province, College of Optoelectronic Engineering, Shenzhen University, 518060, Shenzhen, China

[c] School of Materials Science and Engineering, Nanjing Institute of Technology, Nanjing 211167, China

[d] Institute of Acoustics, Chinese Academy of Sciences, 100190, Beijing, China

[e] School of Optical and Electronic Information, Huazhong University of Sciences and Technology, 1037 Luoyu Road, Wuhan, Hubei 430074, China

[f] School of Materials Science and Engineering, State Key Laboratory of Powder Metallurgy, Central South University, Changsha 410083, China

[g] Faculty of Engineering and Environment, Northumbria University, Newcastle upon Tyne, NE1 8ST, UK

*Corresponding author: luojt@szu.edu.cn (JT. Luo), wangwenwq@mail.ioa.ac.cn (W. Wang)

Highlights

1. Small-size and high-crystallinity PbS CQDs were synthesized via a simple cation exchange method.

2. The PbS CQDs was successfully integrated into the SAW delay lines as the sensing layer by spin-coating at room temperature.

3. The CQD-coated SAW sensor exhibited high sensor response to low-concentration of NO_2 gas with fast response and recovery times at room temperature.

ABSTRACT: Surface acoustic wave (SAW) sensors have great advantages in real-time and *in-situ* gas detection due to their wireless and passive characteristics. Using nanostructured sensing materials to enhance the SAW sensor's responses has become a research focus in recent years. In this paper, solution-processed PbS colloidal quantum dots (CQDs) were integrated into quartz SAW devices for enhancing the performance of NO_2 detection operated at room temperature. The PbS CQDs were directly spin-coated onto ST-cut quartz SAW delay lines, followed by a ligand exchange treatment using $Pb(NO_3)_2$. Upon exposure to 10 ppm of NO_2 gas, the sensor coated with untreated PbS CQDs showed response and recovery times of 487 s and 302 s, and a negative frequency shift of -2.2 kHz, mainly due to the mass loading effect caused by the absorption of NO_2 gas on the surface of the dense CQD film. Whereas the $Pb(NO_3)_2$-treated sensor showed fast response and recovery times of 45 s and 58 s, and a large positive frequency shift of 9.8 kHz, which might be attributed to

the trapping of NO_2 molecules in the porous structure and thus making the film stiffer. Moreover, the $Pb(NO_3)_2$-treated sensor showed good stability and selectivity at room temperature.

Keywords: Surface acoustic wave; Gas sensor; Colloidal Quantum dots; Nitrogen oxide; Lead sulfide

1. Introduction

Surface acoustic wave (SAW) devices have received extensive interest for sensor applications owing to their small size, high sensitivity and ability to interface with passive wireless systems [1-6]. SAW devices can be developed into highly sensitive sensors for continuously monitoring of hazardous and flammable gases in the sub-ppm regime if integrating with specifically designed sensing materials which are sensitive to a certain type of gas. In this case, the sensing material interacts with the target gas molecules and causes detectable changes in the acoustic wave velocity or amplitude, which are then manifested as a frequency/phase angle shifts or insertion loss [7].

In the past decade, considerable attention has been paid to SAW gas sensors by utilizing a variety of materials as sensing layers, such as polymers [8-10], metal oxides and its nanostructures [11-15] and various carbon-based nanomaterials (e.g.,

graphene, carbon nanotubes) [16-18]. However, majority of these materials have either poor sensing responses at room temperature or long response and recovery times (normally longer than a few minutes), thereby limiting their practical real-time and *in-situ* sensing applications. For instance, a SAW sensor coated with nanocomposites of polymers and ordered mesoporous carbon showed a weak frequency shift (i.e., sensing response) of approximately 0.445 kHz when exposed to 16 ppm of NH_3 at room temperature [9]. A Love-wave SAW sensor using graphene oxide as the sensing layer was developed for detection of chemical warfare agent stimulants, and a frequency shift of 0.760 kHz when exposed to 1 ppm of DMMP was obtained [16]. A SAW sensor containing composite films of graphene–nickel–L-alanine had a response of 0.667 kHz when exposed to 200 ppm of CO_2 gas at a high operating temperature of 200 ^oC [17]. The limited responses of these sensors are mainly explained by that their sensing mechanisms were mainly dominated by the mass-loading effects, in which a minor increase in the coverage area of the sensing films would not cause a significant frequency shift. Compared with polymers and carbon-based nanomaterials, metal oxide-based SAW gas sensors exhibited higher responses. Luo et al. and Tang et al. reported SAW gas sensors using SnO_2 [19] and Co_3O_4/SiO_2 composite films [20] based on the mechanism of frequency peak shift due to the conductance changes, and relatively higher response (more than 3 $kHz \cdot ppm^{-1}$) were obtained. However, the slow response and recovery process remained problems to be solved. Gupta et al. prepared a ZnO/Quartz SAW sensor for NO_2 gas detection with a frequency shift as high as 6-112 kHz within 0.04-16 ppm

levels [21]. The dynamic response and recovery characteristics, however, have not been studied. Therefore, the development of room temperature SAW gas sensors with a high response, fast response and recovery times and excellent cross-selectivity is still challenging.

Colloidal quantum dots (CQDs) are attractive materials in thin-film optoelectronic devices, which have been commonly used as photodetectors, solar cells, lasers and light emitting diodes [22-25]. The ever-growing interest in CQDs derives from the benefits in their facile solution processability, low material cost, and unique chemical and physical properties that enable tunable functionality [26]. Additionally, since the CQDs are nanocrystals of a few nanometers in diameter, they have large surface-to-volume ratios that provide plenty of active sites for the absorption of target gas molecules. Their crystal sizes are comparable with the Debye length, which favors fast transfers of the generated charges thus increasing the gas responses. These features open another field for using the CQDs into high-performance gas sensors. Recently, metal chalcogenide and oxide CQDs used in chemiresistive gas sensors have been reported to exhibit enhanced sensing responses towards NO_2 and H_2S gases at room temperature [27-32]. Nonetheless, to the best of our knowledge, there are not many studies towards the integration of CQDs with SAW devices for gas detection.

In this paper, for the first time, we demonstrated the potential of using PbS CQDs as a sensing layer on SAW devices for achieving a ppb-level detection limit of NO_2 gas at room temperature. Owing to the facile solution processability, thin films with PbS CQDs were fabricated directly from the solution phase by spin coating PbS

CQDs onto a two-port SAW delay line. In this process, the highly crystalline CQDs did not require high sintering temperatures or strict deposition conditions to finely control the film crystallization, which was reported critical for the fabrication of metal oxide-based SAW gas sensors using sol-gel or magnetron sputtering [33,21]. The shift of the SAW frequency was precisely measured by varying concentrations of NO_2 gas molecules from 500 ppb to 30 ppm at room temperature. In addition, the gas-sensing mechanisms of the CQD-based SAW gas sensors were investigated.

2. Experimental details

2.1 Synthesis of PbS CQDs

In our previously reported work of PbS CQD-based chemiresistive gas sensors [28,29], the CQDs were synthesized through the reaction of lead oleate and bis(trimethylsilyl) sulfide (TMS). However, TMS is malodorous and easily oxidized, thus a glove box is always required for its manipulation, making this type of synthesis inconvenient. In this study, we used a cation-exchange route developed by Zhang et al. [34] to synthesize the PbS CQDs without the use of a glove box and TMS. Briefly, the $(NH_4)_2S$/OLA solution was injected into Cd-oleate to obtain CdS CQDs. Then, PbS CQDs were formed by the rapid injection of CdS CQDs into a pre-heated $PbCl_2$-OLA solution that promoted direct exchange of Cd^{2+} cation for Pb^{2+} cation. In a typical synthesis, 0.28 g of CdO, 1.8 g of oleic acid (OA), and 8 g of 1-octodecene (ODE) were heated at 260 ^oC for 20 min to form the Cd precursor. Then, the solution was cooled down to 30 ^oC. Meanwhile, the S precursor was prepared by dispersing a 360 μL $(NH_4)_2S$ aqueous solution into 10 mL of oleylamine (OLA). The S precursor

solution was injected into the Cd precursor solution at 30 ^{o}C and then was stirred for 1 hour without heating. The CdS CQDs were washed twice using hexane and ethanol and dispersed in toluene. After that, the Pb precursor was obtained by heating 1.5 mmol $PbCl_2$ in 5 mL of OLA at 140 ^{o}C for 30 min, until a white and turbid solution formed. Then, 5 mL of CdS CQDs in the ODE (20 mL) was injected swiftly into the Pb precursor solution at 140 ^{o}C. About thirty seconds after, the reaction was quenched using a cool water bath, and 5 mL of hexane and 4 mL of OA were added at 70 ^{o}C and 40 ^{o}C, respectively. Finally, the PbS CQDs were washed twice using hexane and ethanol, respectively, and then dispersed in octane at a concentration of 30 mg/mL.

2.2 SAW gas sensor fabrication

The structure of the SAW gas sensor is shown in Fig. 1. Two-port SAW delay lines, consisted of the input and output interdigital transducers (IDTs), were fabricated on ST-cut quartz crystal using a conventional photolithography technology. The IDTs had a periodicity of 15.8 μm and were formed using a magnetron sputtered aluminum layer with a thickness of 200 nm. PbS CQDs were coated onto the entire surface area of the SAW delay lines using a spin-coating process, followed by a ligand exchange treatment. Typically, in this process, a few drops of CQD solution were spun coated onto the SAW device at 2000 rpm for 30 s. Then, the diluted $Pb(NO_3)_2$ in methanol (10 mg/mL) was dropped onto the film within 45 s, and then spun at 2000 rpm for 30 s. The $Pb(NO_3)_2$ treatment was repeatedly deposited onto the device surface twice. Finally, the film was washed using absolute methanol twice in order to remove residues.

2.3 Characterization

High-resolution transmission electron microscopy (HRTEM) images were recorded using a JEOL-2100 microscope operating at an accelerating voltage of 200 kV. X-ray diffraction (XRD) pattern was recorded using a diffractometer (MAXima XXRD-7000, Shimadzu, Japan) with Cu Kα radiation in the 2θ range of 10-80°. UV-vis absorption spectra were measured using a PerkinElmer Lambda 950 UV/vis/NIR spectrophotometer. Fourier transform infrared (FTIR) spectra was obtained using a Bruker Vertex 70 infrared spectrometer. Scanning electron microscope (SEM) characterization was carried out using a Zeiss Supra 55 microscope.

2.4 Sensor characterization

The experimental setup for the gas measurement is shown in Fig. 2. The SAW sensor was assembled onto a specially designed printed circuit board (PCB) and then mounted inside a testing chamber with a volume of 1 L. The humidity and temperature in the chamber, measured by a hygrothermograph (Sensirion, EK-H4), were maintained at 45% and 25 °C, respectively, using an air conditioner. NO_2 gas with the desired concentrations determined by the volume ratio was injected into the chamber using syringes. The sensors responses, given by frequency shifts, were measured using a network analyzer (Keysight, E5071C).

3. Results and discussion

TEM images in Fig. 3a and Fig. 3b show that the prepared PbS CQDs were uniformly distributed and nearly spherically shaped particles with sizes about 4.5±0.3 nm. A

representative HRTEM image of the sample (Fig. 3c) shows lattice fringes with interplanar spacings of 0.343 nm and 0.297 nm, corresponding to the (111) and (200) facets of PbS, respectively. The six diffraction rings are clearly observed in the selected area electron diffraction (SAED) pattern in Fig. 3d, suggesting a high degree of crystallinity. XRD pattern of the CQD (Fig. 4a) can be indexed as the cubic-lattice PbS (JCPDS 05–0592), which is in a good agreement with the results reported by the Zhang group [34]. The broad peaks were attributed to the small size of the CQDs. No peaks assigned to CdS were found in the PbS CQDs, indicating the complete exchange from CdS to PbS. In the UV-vis absorption spectra (Fig. 4b), the PbS CQDs exhibit the first exciton absorption peak at ~1246 nm, corresponding to a significantly widened bandgap (E_g) of 1.0 eV when compared to the bulk bandgap (0.41 eV) of PbS. The diameter (d) of the CQDs was calculated to be 4.52 nm according to the empirical equation reported by Moreels [35]:

$$E_g = 0.41 + (0.0252d^2 + 0.283d)^{-1} \quad (1)$$

The calculated result is in good agreement with the HRTEM results. All these results indicated that the prepared PbS CQDs are small in size and highly crystallized.

After spin-coating at room temperature in ambient air to form a PbS CQD film on the SAW device, we applied a film-level soaking treatment using $Pb(NO_3)_2$ to exchange the long-chain surface-capping ligands of oleic acid and oleylamine, which otherwise would create an insulating shell around the CQDs that militate against efficient gas adsorption. The transmission coefficient (S_{21}) responses of the SAW devices before and after coated with PbS CQDs were measured and the results are

shown in Fig. 5. The measured center frequency of the uncoated device is 200 MHz and the insertion loss is -11.7 dB. After depositing the CQD layer, the center frequency and the corresponding insertion loss of the SAW device are decreased to 199.9 MHz and -12.7 dB respectively, which was due to the mass (PbS CQD) loading effect [36]. When the sensor was further treated with $Pb(NO_3)_2$, no apparent changes in either center frequency or insertion loss were observed. The above results indicated that the integration of PbS CQDs on the SAW delay line did not cause significant changes to the device characteristics, allowing further gas sensing experiments.

Figure 6 shows the representative response curves of the SAW sensors integrated with the untreated and $Pb(NO_3)_2$-treated PbS CQD films exposed to 10 ppm of NO_2 gas at room temperature. It can be observed that the sensor coated with the untreated film showed a negative response of around -2.2 kHz. The frequency was decreased to reach 90% of its saturated level within 487 s and gradually returned to 10% of its maximal value after 302 s, indicating a full recovery. Interestingly, the sensor coated with the $Pb(NO_3)_2$-treated film exhibited a positive response of 9.8 kHz and a much faster response/recovery time (45 s/58 s) than that of the untreated one. To explain the observed opposite sensor response, we investigated the sensing mechanism of our PbS CQD-based SAW gas sensors as follows.

Generally, the origin of the frequency shift in SAW gas sensors depends mainly on the following three factors: mass loading, changes in elasticity and acousto-electric interaction. The equation representing these three contributions is given as [37]:

$$\frac{\Delta f}{f_0} \cong \frac{\Delta v}{v_0} = -C_m f_0 \Delta(\rho_s) + 4C_e f_0 \Delta(hG') - \frac{K^2}{2}\Delta\left(\frac{1}{1+\left(\frac{v_0 c_s}{\sigma_s}\right)^2}\right) \quad (2)$$

where Δf and f_0 are the frequency shift and the initial center frequency, Δv and v_0 are the change in SAW velocity and unperturbed SAW velocity, C_m and C_e are the sensitivity coefficients of mass and elasticity respectively, ρ_s and h are the density per unit area and the thickness of the sensing layer respectively, G' is the shear modulus, K^2 is the electromechanical coupling coefficient, σ_s is the sheet conductivity of the sensing layer, c_s is the capacitance per unit length of the device. In Eq. (2), the first term and the third term represent effects of the changes in mass and electrical conductivity of the sensing film, respectively. These two effects both result in a negative change of the center frequency (e.g., a decrease in frequency). The second term is contributed from the changes in elasticity, which results in a positive change of the center frequency (e.g., a increase in frequency).

For the untreated PbS/SAW gas sensor, the center frequency decreased after the supply of NO_2 gas. According to Eq. (2), both mass loading effect and acousto-electric interaction may cause the decrease in frequency. In order to separate the contributions of mass loading and acousto-electric interaction, an Al film with a thickness of 120 nm was deposited on the sensing area of the SAW delay line using magnetron sputtering before the addition of the PbS CQD film. The SAW sensor with Al film would only sense non-electrical signal changes, since the metal film can eliminate the acousto-electric effect [38]. The mechanical effects, such as mass loading, would not be affected by the deposition of the Al film. After the PbS CQD film was added, the reference sensor (with Al film) and a standard sensor (without Al film) were then exposed to 10 ppm of NO_2 for comparison. As shown in Fig. 7, the

two sensors exhibit almost the same frequency shift, suggesting that the sensing response was not suppressed by the intervening Al layer. Hence, it could be inferred from the comparison experiment that the acousto-electric interaction did not play a significant role in the observed sensing response. On the other hand, it should be noted that the effect of acousto-electric interaction is related to the change in conductivity of the sensing film. Therefore, to further identify the small contribution of acousto-electric interaction, the sheet conductivity (σ_s = 4.8×10^{-8} S·cm^{-1}) of the untreated PbS CQD film was obtained by Hall effect measurement. In the third term of Eq. (2), the calculated value of $(v_0c_s/\sigma_s)^2$ is « 1 (c_s = 0.5 pF·cm^{-1}, v_o=3158 m·s^{-1} for substrate of ST-cut quartz). Meanwhile, the K^2 of the ST-cut quartz substrate has a low value of 0.11%.Thus, it can be concluded that acousto-electric interaction have a negligible contribution to the sensing response. The Δf is mainly caused by the mass loading effect for the untreated PbS/SAW gas sensor.

To further understanding the role of the $Pb(NO_3)_2$ treatment on the sensing mechanism, we conducted the FTIR analysis and the results are shown in Fig. 8a. As observed, the intensity characteristics of the transmittance peaks (2850–2920 cm^{-1}) for the aliphatic C–H stretching bands are significantly decreased, indicating that $Pb(NO_3)_2$ treatment could remove most of the OA and OLA ligands around the CQDs through a ligand exchange process (Fig. 8b). It should be noted that the removal of these OA and OLA ligands would induce volume shrinkage in the CQD films, and thus some small cracks are formed after the $Pb(NO_3)_2$ treatment as shown in the top-view SEM images (Fig. 9). The presence of these small cracks should provide

more areas for the target gas (NO_2) molecules to be adsorbed. More and more NO_2 molecules will be bounded to the crack walls and condensed in the cracks, which could result in an increase in the stiffness in the sensing layer and thereby increase the SAW frequency [39]. Therefore, we believe that the changes in elasticity are the dominant sensing mechanism for $Pb(NO_3)_2$-treated PbS/SAW gas sensor. The increase in elasticity of the sensing film due to the entrapment of target gas molecules in pores at grain boundaries was also reported by other researchers [40,41].

Based on the above discussions, we propose a model for the sensing mechanism of PbS CQD-based SAW gas sensors in the present work (Fig. 10). The spin-coating of PbS CQDs onto the SAW device result in a dense film after the solvent volatilization. Upon exposure to NO_2 atmosphere, the NO_2 molecules are physically absorbed on the surface of the CQD film and induce an increase in the film mass, which hinders the acoustic wave propagation and also results in a decrease in the center frequency due to the mass-loading effect as shown in Fig. 10. When the sensor was treated by $Pb(NO_3)_2$, the long-chain ligands around the CQDs are removed and some small cracks are appeared on the film surface. In this case, large amounts of NO_2 molecules are trapped in the cracks as shown in Fig. 10. As a result, the sensing film becomes stiffer. Consequently, the center frequency increased due to the increase in elasticity. Furthermore, the porous morphology of the $Pb(NO_3)_2$-treated film enables rapid gas adsorption and diffusion, thus resulting in faster response and recovery times than those of the untreated device.

To investigate the potential practical applications of the $Pb(NO_3)_2$-treated sensor, its

detection limits, stability and selectivity were further studied. As shown in Fig. 11a, the dynamic sensing responses of the sensor toward different concentrations of NO_2 gas were measured at room temperature. Upon exposure to NO_2, the response increased from 1 to 12 kHz with changes in the NO_2 concentration from 0.5 to 30 ppm. The response was found to be linearly proportional to the NO_2 concentration in the region below 10 ppm (Fig. 11b). The slope in the linear regime was 0.91 ppm^{-1} with a fitting quality R^2=0.997. Using the least-square method of fitting in the linear regime [42], we estimated the theoretical detection limit (DL) for NO_2 gas as follows: 200 data points at the initial baseline in Fig. 11a were taken. These points were then averaged and a standard deviation (S) was obtained to be 0.14 kHz. Thus the sensor noise (RMS_{noise}) was calculated to be 0.01 using the root-mean-square deviation (RMSD) according to the Eq. (3) and the theoretical detection limit is about 32 ppb according to the Eq. (4).

$$RMS_{\text{noise}} = \sqrt{\frac{S^2}{\text{N}}} \tag{3}$$

$$\text{DL(ppm)} = 3\frac{RMS_{noise}}{\text{Slope}} \tag{4}$$

where N is the number of data points. This ppb level of the detection limit for NO_2 gas suggested the potential usage of our $Pb(NO_3)_2$-treated PbS SAW sensor in applications of environmental monitoring and breath analysis, especially for diagnosing asthma. To test the stability, the sensor was exposed to 10 ppm of NO_2 gas for three consecutive cycles (Fig. 11c). The frequency shift was highly reproducible, and a standard deviation of ~54 Hz was found for the successive exposures. Moreover, to evaluate the selectivity of the sensor, we conducted gas-sensing tests towards

various gas species, i.e., H_2S, NH_3, H_2 and ethanol. The sensor showed superior selectivity towards NO_2 gas ($\triangle f$ = 10 kHz at 10 ppm) against other interfering gases ($\triangle f$ < 0.6 kHz at 100 ppm) (Fig. 11d). Considering this result, the sensor is capable of selectively detecting NO_2 gas in a complex atmosphere. Eventually, we summarized the performance of our PbS CQD-based SAW gas sensor and compared it with other SAW NO_2 gas sensors reported in the literatures (**Table 1)**. The results indicated that our sensor exhibited a sensitive response at lower concentration, fast response and recovery times as well as low working temperature, capable of being a potential application in portable devices with low power consumption. Moreover, the sensor was made by spin-coating a CQD film onto SAW device, a simple and cost-effective approach compared to magnetron sputtering or pulsed laser deposition.

4. Conclusions

In this work, we demonstrated for the first time that PbS CQDs synthesized via a cation-exchange method could be successfully integrated into a SAW delay line as the sensing layer for highly sensitive NO_2 detection. The sensor coated with the untreated PbS CQDs had a dense film morphology and showed a negative response, which was mainly due to the increase in the mass loading caused by absorbed NO_2 gas. In contrast, the sensor coated with the $Pb(NO_3)_2$-treated PbS CQDs had a porous film morphology with some small cracks and showed a positive response. These small cracks appeared to favor a change in the elasticity of the sensing layer with exposure to NO_2 gas. Moreover, the $Pb(NO_3)_2$-treated sensor showed a potential for monitoring traces of NO_2 (0.5–30 ppm) with good sensitivity and selectivity at room temperature.

Acknowledgment

The authors gratefully acknowledge the support of Research and Development Program of China (Grant no. 2016YFB0402705), National Natural Science Foundation of China (Grant no. 11704261, 11575118), Natural Science Foundation of SZU (Grant no. 2017067), Shenzhen Key Lab Fund (ZDSYS20170228105421966), Shenzhen Science & Technology Project (Grant no. JCYJ20170817100658231), the Fund for Research and Development of Science and Technology of Shenzhen (Grant no. JCYJ20160414102255597), PhD Start-up Fund of Natural Science Foundation of Guangdong Province, China (2017A030310375). Funding supports from UK Engineering Physics and Science Research Council (EPSRC EP/P018998/1), Newton Mobility Grant (IE161019) through Royal Society and NFSC, and Royal academy of Engineering UK-Research Exchange with China and India are acknowledged.

References

[1] L. Rana, R. Gupta, M. Tomar, V. Gupta, Highly sensitive Love wave acoustic biosensor for uric acid, Sensors and Actuators B-Chemical 261 (2018) 169-177.

[2] Z. Xu, Y. J. Yuan, Implementation of guiding layers of surface acoustic wave devices: A review, Biosensors & Bioelectronics 99 (2018) 500-512.

[3] H. S. Xu, S. R. Dong, W. P. Xuan, U. Farooq, S. Y. Huang, M. L. Li, T. Wu, H. Jin, X. Z. Wang, J. K. Luo, Flexible surface acoustic wave strain sensor based on single crystalline $LiNbO_3$ thin film, Applied Physics Letters 112 (2018) 093502.

[4] J. T. Luo, N. R. Geraldi, J. H. Guan, G. Mchale, G. G. Wells, Y. Q. Fu, Slippery liquid-infused porous surfaces and droplet transportation by surface acoustic waves, Physical Review Applied 7 (2017) 014017.

[5] J. T. Luo, F. Pan, P. Fan, F. Zeng, D. P. Zhang, Z. H. Zheng, G. X. Liang, Cost-effective and high frequency surface acoustic wave filters on ZnO:Fe/Si for low -loss and wideband application, Applied Physics Letters 101 (2012) 172909.

[6] J. T. Luo, F. Pan, P. Fan, F. Zeng, D. P. Zhang, Z. H. Zheng, G. X. Liang, X. M. Cai, Effects of Mn-doping on surface acoustic wave properties of ZnO films, Physica Status Solidi-Rapid Research Letters 6 (2012) 436-438.

[7] A. Afzal, N. Iqbal, A. Mujahid, R. Schirhagl, Advanced vapor recognition materials for selective and fast responsive surface acoustic wave sensors: A review, Analytica Chimica Acta 787 (2013) 36-49.

[8] R. D. S. Yadava, V. K. Verma, A diffusion limited sorption–desorption noise model for polymer coated SAW chemical sensors, Sensors and Actuators B-Chemical 195 (2014) 590-602.

[9] P. H. Ku, C. Y. Hsiao, M. J. Chen, T. H. Lin, Y. T. Li, S. C. Liu, K. T. Tang, D. J. Yao, C. M. Yang, Polymer/ordered mesoporous carbon nanocomposite platelets as superior sensing materials for gas detection with surface acoustic wave devices, Langmuir 28 (2018) 11639-11645.

[10] X. Chen, D. M. Li, S. F. Liang, S. Zhan, M. Liu, Gas sensing properties of surface acoustic wave NH_3 gas sensor based on Pt doped polypyrrole sensitive film, Sensors and Actuators B-Chemical 121 (2013) 364-369.

[11] Y. L. Tang, Z. J. Li, J. Y. Ma, Y. J. Guo, Y. Q. Fu, X. T. Zu, Ammonia gas sensors based on ZnO/SiO_2 bi-layer nanofilms on ST-cut quartz surface acoustic wave devices, Sensors and Actuators B-Chemical 201 (2014) 114-121 .

[12] Y. L. Tang, D. Y. Ao, W. Li, X. T. Zu, S. Li, Y. Q. Fu, NH_3 sensing property and mechanisms of quartz surface acoustic wave sensors deposited with SiO_2, TiO_2, and SiO_2-TiO_2 composite films, Sensors and Actuators B-Chemical 254 (2018) 1165-1173.

[13] L. Yang, C. B. Yin, Z. L. Zhang, J. J. Zhou, H. H. Xu, The investigation of hydrogen gas sensing properties of SAW gas sensor based on palladium surface modified SnO_2 thin film, Materials Science in Semiconductor Processing, 60 (2017) 16-28.

[14] Y. L. Tang, Z. J. Li, J. Y. Ma, L. Wang, J. Yang, B. Du, Q. K. Yu, X. T. Zu, Highly sensitive surface acoustic wave (SAW) humidity sensors based on sol-gel SiO_2 films: Investigation on the sensing property and mechanism, Sensors and Actuators B-Chemical 215 (2015) 283-291.

[15] S. Y. Wang, J. Y. Ma, Z. J. Li, H. Q. Su, N. R. Alkurd, W. L. Zhou, L. Wang, B. Du, Y. L. Tang, D. Y. Ao, S. C. Zhang, Q. K. Yu, X. T. Zu, Surface acoustic wave ammonia sensor based on ZnO/SiO_2 composite film, Journal of Hazardous Materials 285 (2015) 368-374.

[16] I. Sayago, D. Matatagui, M. J. Fernández, J. L. Fontecha, I. Jurewicz, R. Garriga, E. Muñoz, Graphene oxide as sensitive layer in Love-wave surface acoustic wave sensors for the detection of chemical warfare agent simulants,

Talanta 148 (2016) 393-400.

[17] S. Xu, C. P. Li, H. J. Li, M. J. Li, C. Q. Qu, B. H. Yang, Carbon dioxide sensors based on a surface acoustic wave device with a graphene–nickel–L-alanine multilayer film, Journal of Materials Chemistry C 3 (2015) 3882-3890.

[18] Y. Z. Wang, M. K. Chyu, Q. M. Wang, Passive wireless surface acoustic wave CO_2 sensor with carbon nanotube nanocomposite as an interface layer, Sensors and Actuators A: Physical 220 (2014) 34-44.

[19] W. Luo, J. F. Deng, Q. Y. Fu, D. X. Zhou, Y. X. Hu, S. P. Gong, Z. P. Zheng, Nanocrystalline SnO_2 film prepared by the aqueous sol–gel method and its application as sensing films of the resistance and SAW H_2S sensor, Sensors and Actuators B-Chemical 217 (2015) 119-128.

[20] Y. L. Tang, Z. J. Li, J. Y. Ma, H. Q. Su, Y. J. Guo, L. Wang, B. Du, J. J. Chen, W. L. Zhou, Q. K. Yu, X. T. Zu, Highly sensitive room-temperature surface acoustic wave (SAW) ammonia sensors based on Co_3O_4/SiO_2 composite films, Journal of Hazardous Materials 280 (2014) 127-133.

[21] L. Rana, R. Gupta, M. Tomar, V. Gupta, ZnO/ST-Quartz SAW resonator: An efficient NO_2 gas sensor, Sensors and Actuators B-Chemical 252 (2017) 840-845.

[22] R. Saran, R. J. Curry, Lead sulphide nanocrystal photodetector technologies, Nature photonics 10 (2016) 81-92.

[23] R. L. Wang, Y. Q. Shang, P. Kanjanaboos, W. J. Zhou, Z. J. Ning, E. H. Sargent, Colloidal quantum dot ligand engineering for high performance solar cells,

Energy & Environmental Science 9 (2016) 1130-1143.

[24] F. Fan, O. Voznyy, R. P. Sabatini, K. T. Bicanic, M. M. Adachi, J. R. McBride, K. R. Reid, Y. S. Park, X. Y. Li, A. Jain, R. Quintero-Bermudez, M. Saravanapavanantham, M. Liu, M. Korkusinski, P. Hawrylak, V. I. Klimov, S. J. Rosenthal, S. Hoogland, E. H. Sargent, Continuous-wave lasing in colloidal quantum dot solids enabled by facet-selective epitaxy, Nature 544 (2017) 75-79.

[25] X. Dai, Z. Zhang, Y. Jin, Y. Niu, H. Cao, X. Liang, L. Chen, J. Wang, X. Peng, Solution-processed, high-performance light emitting diodes based on quantum dots, Nature 515 (2014) 96-99.

[26] J. Y. Kim, O. Voznyy, D. Zhitomirsky, E. H. Sargent, 25th anniversary article: colloidal quantum dot materials and devices: A quarter-century of advances, Advanced Materials 25 (2013) 4986-5010.

[27] H. Liu, M. Li, O.Voznyy, L. Hu, Q. Fu, D. X. Zhou, Z. Xia, E. Sargent, J. Tang, Physically flexible, rapid-response gas sensor based on colloidal quantum dot solids, Advanced Materials 26 (2014) 2718-2724.

[28] M. Li, D. X. Zhou, J. Zhao, Z. P. Zheng, J. G. He, L. Hu, Z. Xia, J. Tang, H. Liu, Resistive gas sensors based on colloidal quantum dot (CQD) solids for hydrogen sulfide detection, Sensors and Actuators B-Chemical 217 (2015) 198-201.

[29] M. Li, W. K. Zhang, G. Shao, H. Kan, Z. L. Song, S. M. Xu, H. X. Yu, S. L. Jiang, J. T. Luo, H. Liu, Sensitive NO_2 gas sensors employing spray-coated colloidal quantum dots, Thin Solid Films 618 (2016) 271-276.

[30] B. H. Zhang, M. Li, Z. L. Song, H. Kan, H. X. Yu, Q. Liu, G. Z. Zhang, H. Liu, Sensitive H_2S gas sensors employing colloidal zinc oxide quantum dots, Sensors and Actuators B-Chemical 249 (2017) 558-563.

[31] H. Kan, M. Li, Z. L. Song, S. S. Liu, B. H. Zhang, J. Y. Liu, M. Y. Li, G. Z. Zhang, S. L. Jiang, H. Liu, Highly sensitive response of solution-processed bismuth sulfide nanobelts for room-temperature nitrogen dioxide detection, Journal of Colloid and Interface Science 506 (2017) 102-110.

[32] M. Li, J. T. Luo, C. Fu, H. Kan, Z. Huang, W. M. Huang, S. Q. Yang, J. B. Zhang, J. Tang, Y. Q. Fu, H. L. Li, H. Liu, PbSe quantum dots-based chemiresistors for room-temperature NO_2 detection, Sensors and Actuators B-Chemical 256 (2018) 1045-1056.

[33] W. Luo, Q. Y. Fu, D. X. Zhou, J. F. Deng, H. Liu, G. P. Yan, A surface acoustic wave H_2S gas sensor employing nanocrystalline SnO_2 thin film, Sensors and Actuators B-Chemical 176 (2013) 746-752.

[34] J. B. Zhang, B. D. Chernomordik, R. W. Crisp, D. M. Kroupa, J. M. Luther, E. M. Miller, J. B. Gao, M. C. Beard, Preparation of Cd/Pb chalcogenide heterostructured janus particles via controllable cation exchange, ACS Nano 9 (2015) 7151-7163.

[35] I. Moreels, K. Lambert, D. Smeets, D. De Muynck, T. Nollet, J. C. Martins, F. Vanhaecke, A. Vantomme, C. Delerue, G. Allan, Z. Hens, ACS Nano 3 (2009) 3023-3030.

[36] D. Pestov, O. Guney-Altay, N. Levit, G. Tepper, Improving the stability of

surface acoustic wave (SAW) chemical sensor coatings using photopolymerization, Sensors and Actuators B-Chemical 126 (2007) 557-561.

[37] J. D. Gailpeau, R. S. Falconer, J. F. Vetelino, J. J. Caron, E. L. Wittman, M. G. Schweyer, J. C. Andle, Theory, design and operation of a surface acoustic wave hydrogensulfide microsensor, Sensors and Actuators B-Chemical 24–25 (1995) 49-53.

[38] X. D. Wang, W. Wang, H. L. Li, C. Fu, Y. B. Ya, S. T. He, Development of a SnO_2/CuO-coated surface acoustic wave-based H_2S sensor with switch-like response and recovery, Sensors and Actuators B-Chemical 169 (2012) 10-16.

[39] S. L. Hietala, V. M. Hietala, C. J. Brinker, Dual saw sensor technique for determining mass and modulus changes, IEEE Transactions on Ultrasonics, Ferroelectrics, and Frequency Control 48 (2001) 262-267.

[40] V. B. Raj, A. T. Nimal, M. Tomar, M. U. Sharma, V. Gupta, Novel scheme to improve SnO_2/SAW sensor performance for NO_2 gas by detuning the sensor oscillator frequency, Sensors and Actuators B-Chemical 220 (2015) 154-161.

[41] V. B. Raj, H. Singh, A. T. Nimal, M. U. Sharma, M. Tomar, V. Gupta, Distinct detection of liquor ammonia by ZnO/SAW sensor: Study of complete sensing mechanism, Sensors and Actuators B-Chemical 238 (2017) 83-90.

[42] V. Dua, S. P. Surwade, S. Ammu, S. R. Agnihotra, S. Jain, K. E. Roberts, S. Park, R. S. Ruoff, S. K. Manohar, All-organic vapor sensor using inkjet-printed reduced graphene oxide, Angewandte Chemie-International Edition 49 (2010)

2154-2157.

[43] L. Rana, R. Gupta, R. Kshetrimayum, M. Tomar, V. Gupta, Fabrication of surface acoustic wave based wireless NO_2 gas sensor, Surface & Coatings Technology 343 (2018) 89-92.

[44] Y. W. Hu, J. W. Xiang, X. Y. Sun, C. Z. Xu, S. Wang, J. A. Duan, Sensitivity improvement of SAW NO_2 sensors by p-n heterojunction nanocomposite based on MWNTs skeleton, IEEE Sensors Journal 16 (2016) 287-292.

[45] S. Thomas, M. Cole, A. De Luca, F. Torrisi, A. C. Ferrari, F. Udrea, J. W. Gardner, Graphene-coated rayleigh SAW resonators for NO_2 detection, Procedia Engineering 87 (2014) 999-1002.

[46] X. F. Yan, D. M. Li, C. C. Hou, X. Wang, W. Zhou, M. Liu, T. C. Ye, Comparison of response towards NO_2 and H_2S of PPy/TiO_2 as SAW sensitive films, Sensors and Actuators B-Chemical 161 (2012) 329-333.

[47] L. Al-Mashat, H. D. Tran, W. Wlodarski, R. B. Kaner, K. Kalantar-Zadeh, Polypyrrole nanofiber surface acoustic wave gas sensors, Sensors and Actuators B-Chemical 134 (2008) 826-831.

[48] A. Z. Sadek, W. Wlodarski, K. Shin, R. B. Kaner, K. Kalantar-zadeh, A layered surface acoustic wave gas sensor based on a polyaniline/In_2O_3 nanofibre composite, Nanotechnology 17 (2006) 4488-4492.

[49] S. J. Ippolito, S. Kandasamy, K. Kalantar-zadeh, W. Wlodarski, G. Kiriakidis, N. Katsarakis, M. Suchea, Highly sensitive layered ZnO/$LiNbO_3$ SAW device with InO_x selective layer for NO_2 and H_2 gas sensing, Sensors and Actuators

B-Chemical 111 (2005) 207-212.

[50] G. Kiriakidis, K. Moschovis, I. Kortidis, V. Binas, Ultra-low gas sensing utilizing metal oxide thin films, Vacuum 86 (2012) 495-506.

Biographies

Min Li received her Ph.D. degree in School of Optical and Electronic Information from Huazhong University of Science and Technology, China in 2016. She is currently a post-doctor in College of Physics and Energy of Shenzhen University, China. Her research focuses on colloidal quantum dots and thin film gas sensors.

Hao Kan received his Ph.D. degree in School of Optical and Electronic Information from Huazhong University of Science and Technology, China in 2017. He is currently a post-doctor in College of Physics and Energy of Shenzhen University, China. His research focuses on gas sensors and photo-detectors.

Hui Li received her Bachelor's degree in Department of Applied Physics from Tianjin University of Technology and Education, China in 2017. She is currently a Master degree candidate in College of Physics and Energy of Shenzhen University, China. Her research focuses on SAW gas sensors.

Chong Li received his Bachelor's degree in School of Physical and Material Science from He'nan Normal University, China in 2017. He is currently a Master degree candidate in College of Physics and Energy of Shenzhen University, China. His research focuses on SAW biosensors.

Chen Fu received his Bachelor's degree from Chinese University of Geoscience,

Beijing (CUGB) in 2005. In 2011, He received his Ph.D. degree from the Institute of Acoustics (IOA), Chinese Academy of Sciences. Since 2011, he worked as a postdoctoral researcher at Ajou University in South Korea and then at Newcastle university in UK. He now works as an assistant professor at Shenzhen University. His current research interest is on SAW theory and the application of SAW sensors.

Aojie Quan received his Master's degree in College of Physics and Energy of Shenzhen University, China in 2018. He is currently a junior engineer in PCB Piezotronics, Inc. (Beijing), China.

Huibin Sun received his Ph.D. degree in Jilin university in 1990. He is currently an professor in College of Physics and Energy of Shenzhen University, Shenzhen, China.

Xueli Liu received her Master's degree in Ocean University of China, China in 2017. She is currently a Ph.D. degree candidate in Institute of Acoustics from Chinese Academy of Sciences, China. Her research focuses on SAW gas sensors.

Wen Wang received his Master's degree in Central South University in 2002, and his Ph.D. degree from the Institute of Acoustics (IOA), Chinese Academy of Sciences in 2005. From 2005 to 2009 he worked as a postdoctoral researcher and research professor at the microsystem Lab. of Ajou University in South Korea. In 2010, he worked in Freiburg University supported by the Humboldt Foundation as a gust professor. From 2007, he has been associated professor and now acted as professor at the IOA, Chinese Academy of Science, China. His current research involves SAW chemical sensor, SAW gyroscope and SAW biosensor. Prof. Wang was a member of IEEE.

Huan Liu has been an associate professor of School of Optical and Electronic Information at Huazhong University of Science and Technology, China since 2011. She received her Master's degree and Ph.D. degree in micro- and solid-state electronics from Huazhong University of Science and Technology in 2004 and 2008 respectively. From 2009 to 2011, she had been a post-doctoral fellow in the Department of Electrical and Computer Engineering at University of Toronto, Canada. Her research interests include nanostructured functional materials, gas sensors and photovoltaics.

Jingting Luo received the Ph.D. degree from Tsinghua University, Beijing, China, in 2012. From January 2016, he has been working as an academic visitor in Faculty of Engineering and Environment, University of Northumbria at Newcastle, UK. He is currently an associate professor in College of Physics and Energy of Shenzhen University, Shenzhen, China.

List of Figure Captions

Fig. 1. Schematic of the SAW gas sensor.

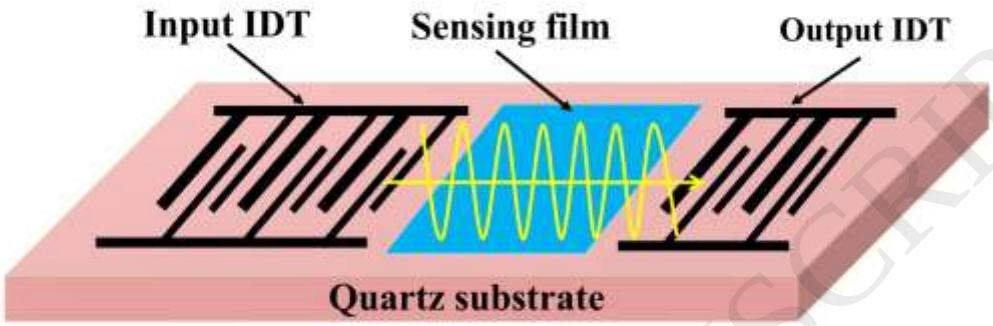

Fig. 2. The setup of the experimental system for gas sensing measurement.

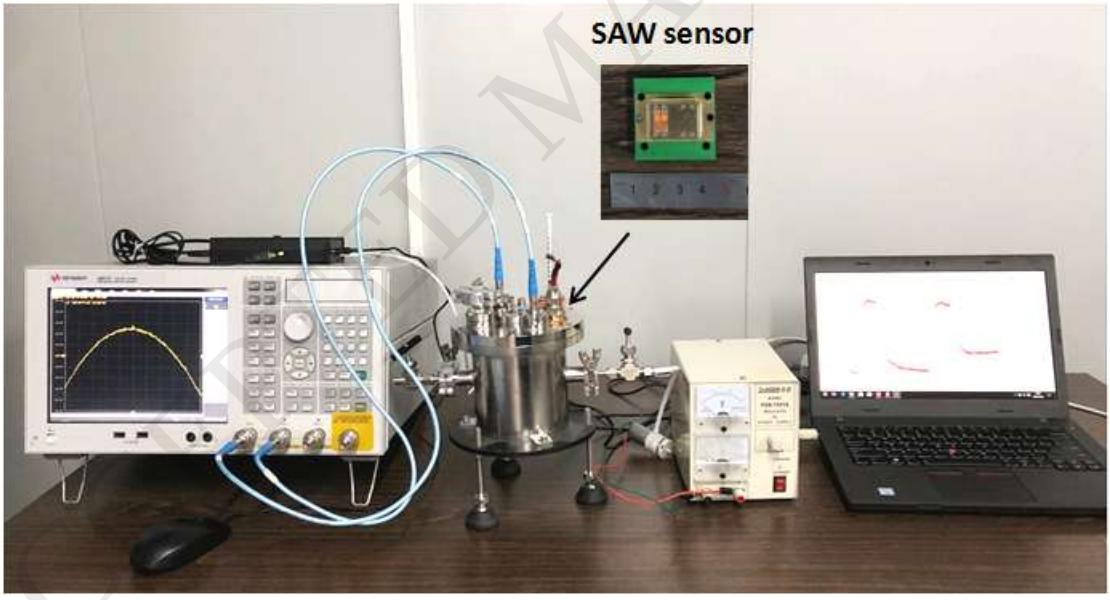

Fig. 3. (a) and (b) Transmission electron microscope (TEM), (c) high-resolution TEM (HRTEM) and (d) selected area electron diffraction (SAED) images of the synthesized PbS CQDs. Inset was the size distribution of the sample.

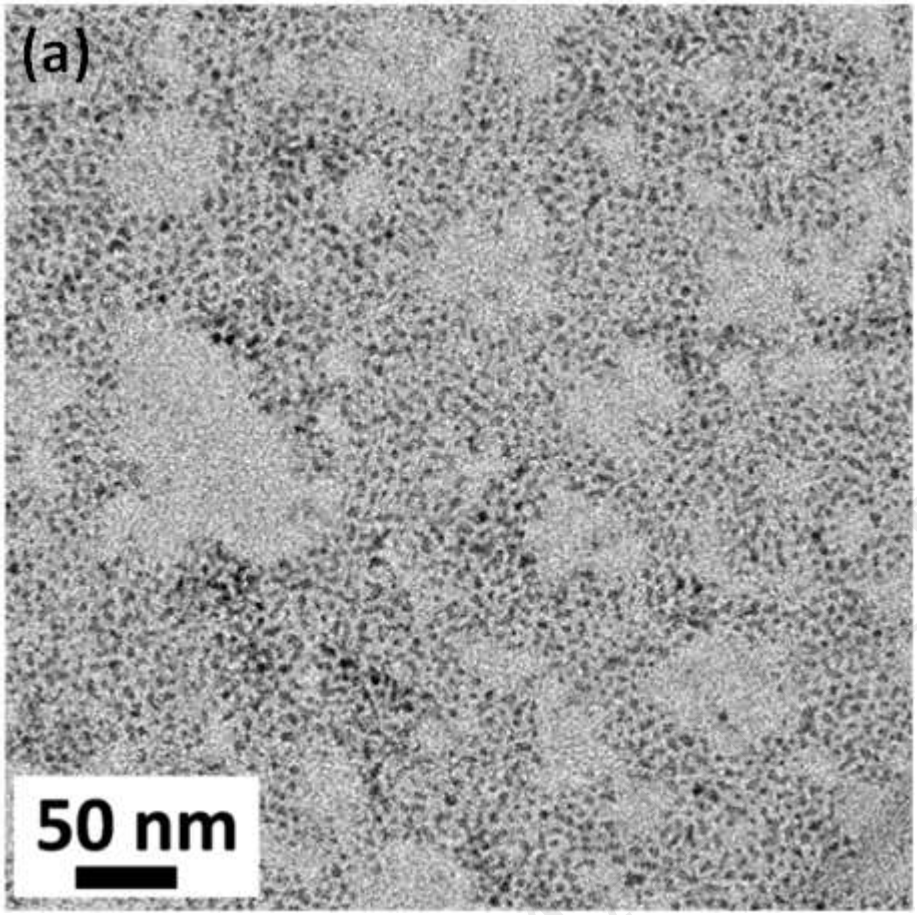

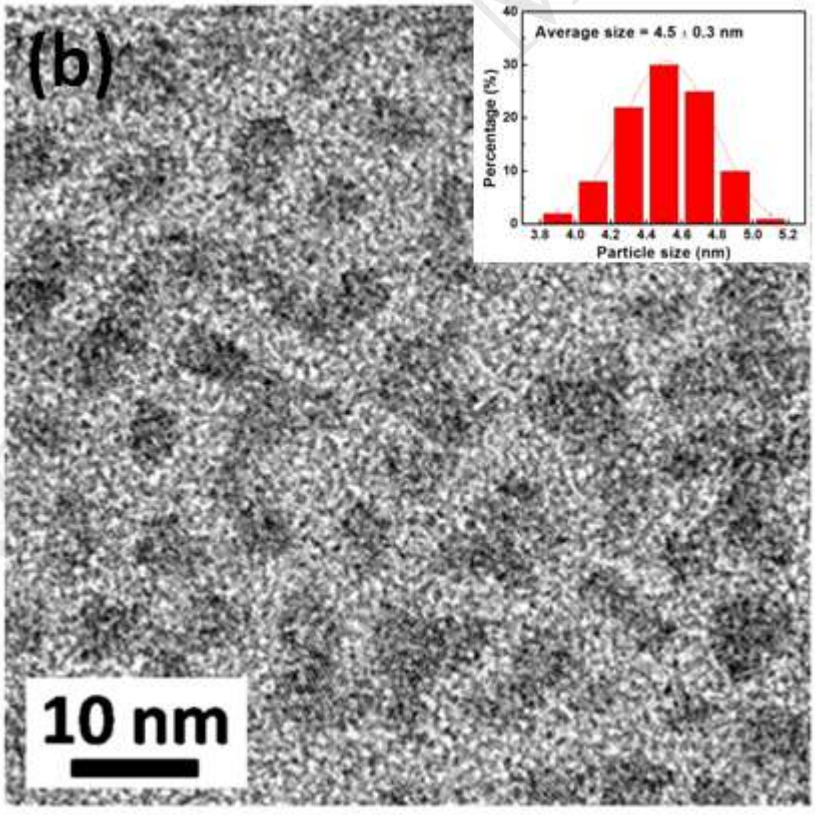

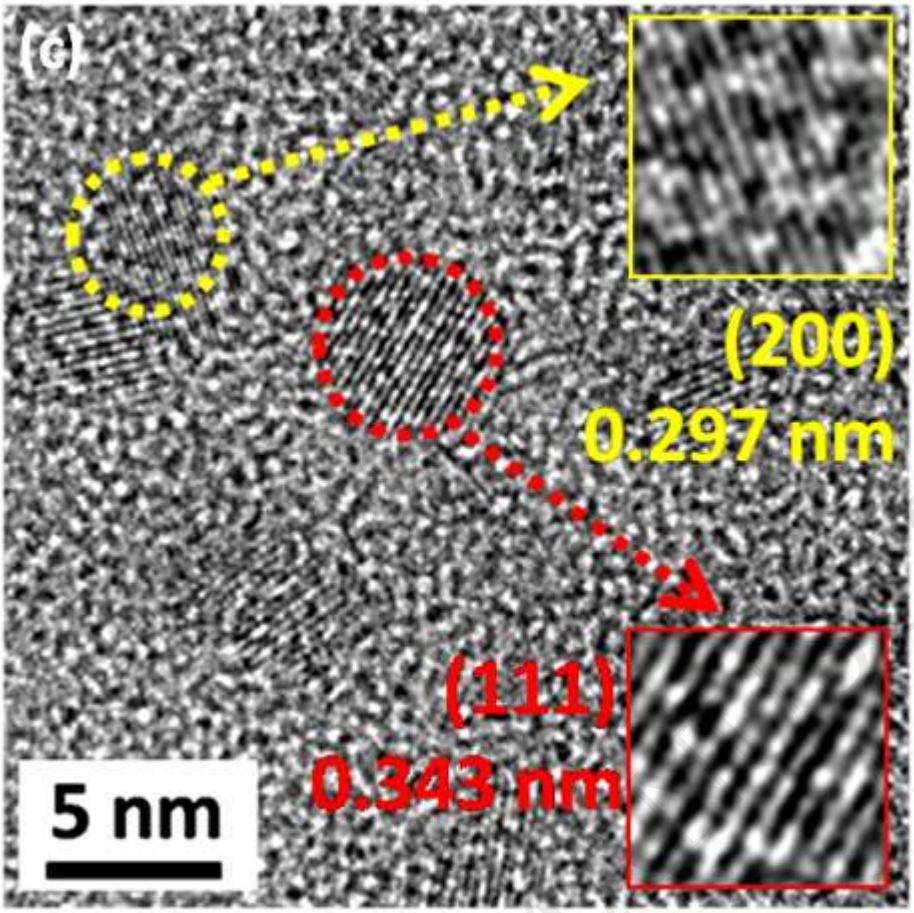

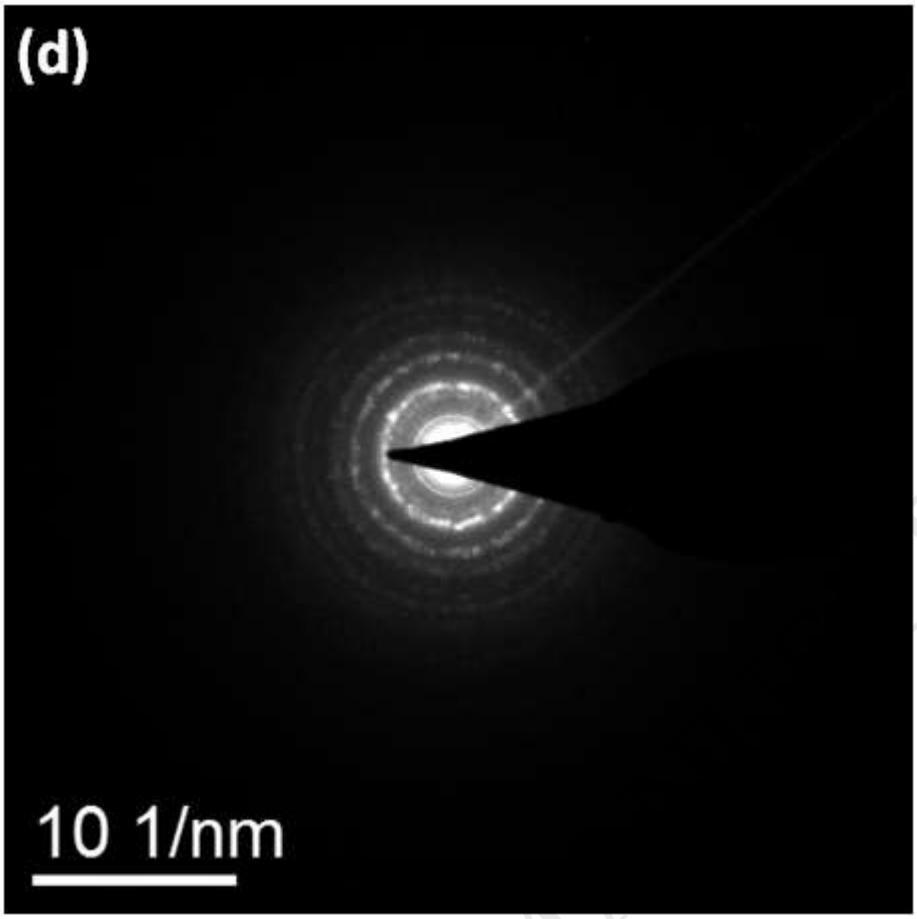

Fig. 4. XRD pattern and UV-vis absorption spectra of the as-prepared PbS CQDs.

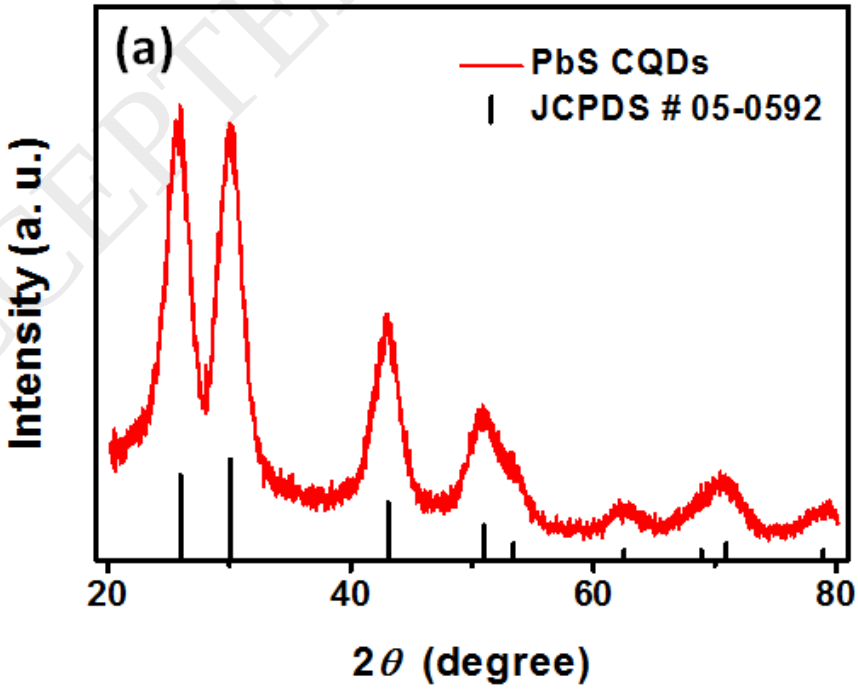

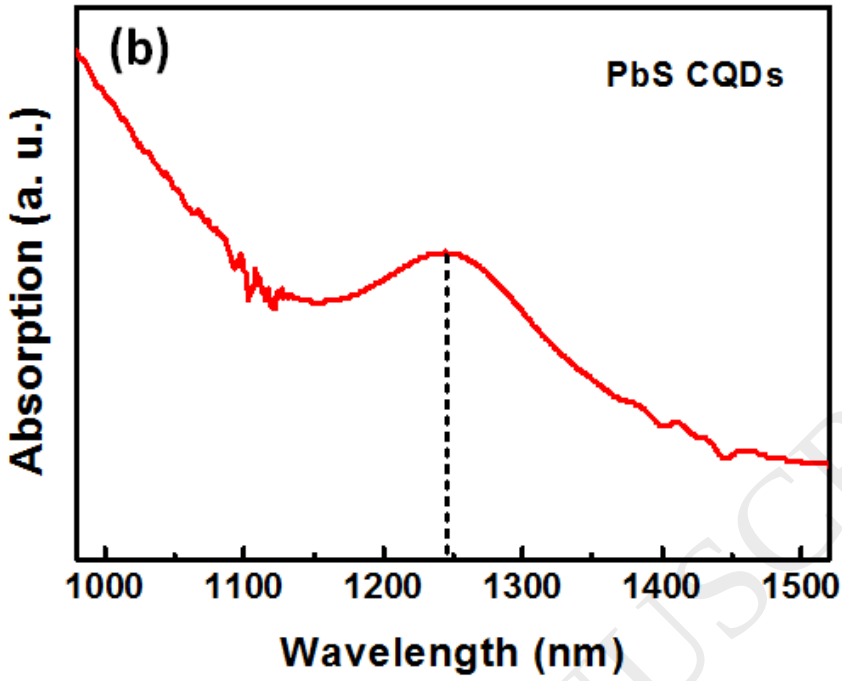

Fig. 5. Frequency response of the SAW devices before and after being coated with ($Pb(NO_3)_2$-treated) PbS CQDs.

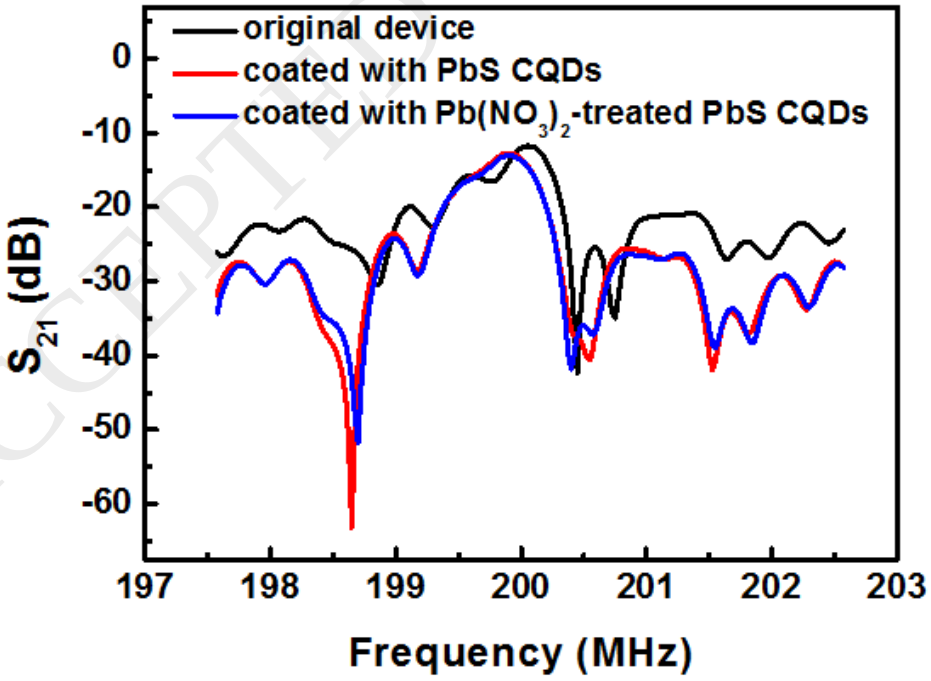

Fig. 6. Response curves of the SAW gas sensors deposited with untreated PbS CQD

film and $Pb(NO_3)_2$-treated PbS CQD film to 10 ppm NO_2.

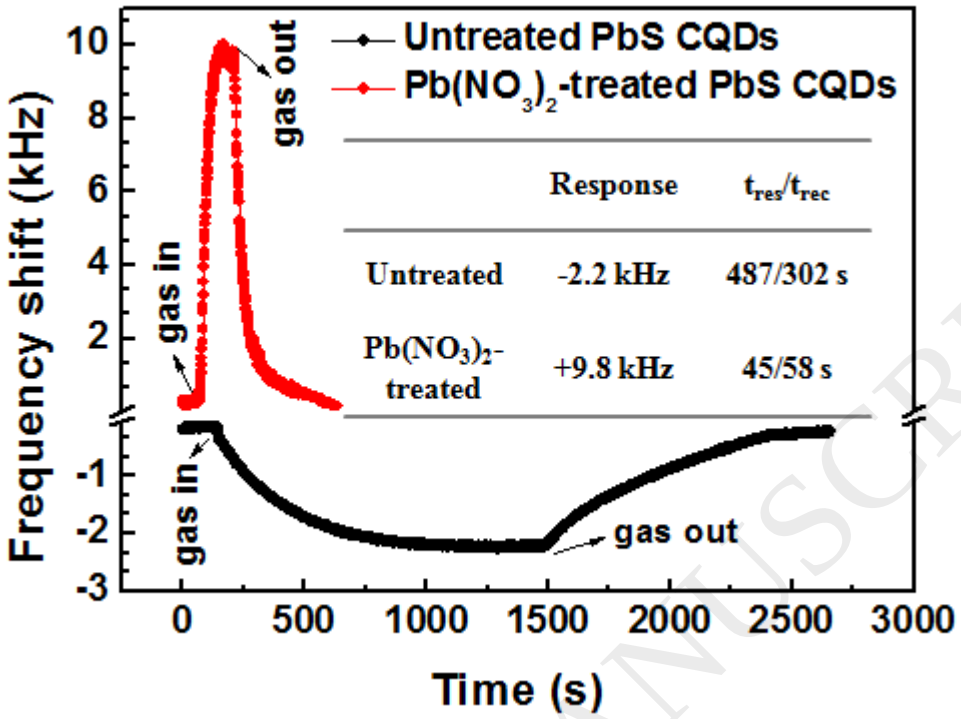

Fig. 7. The frequency response to 10 ppm of NO_2 gas of the normal sensor (without Al film) and contrast sensor (with Al film).

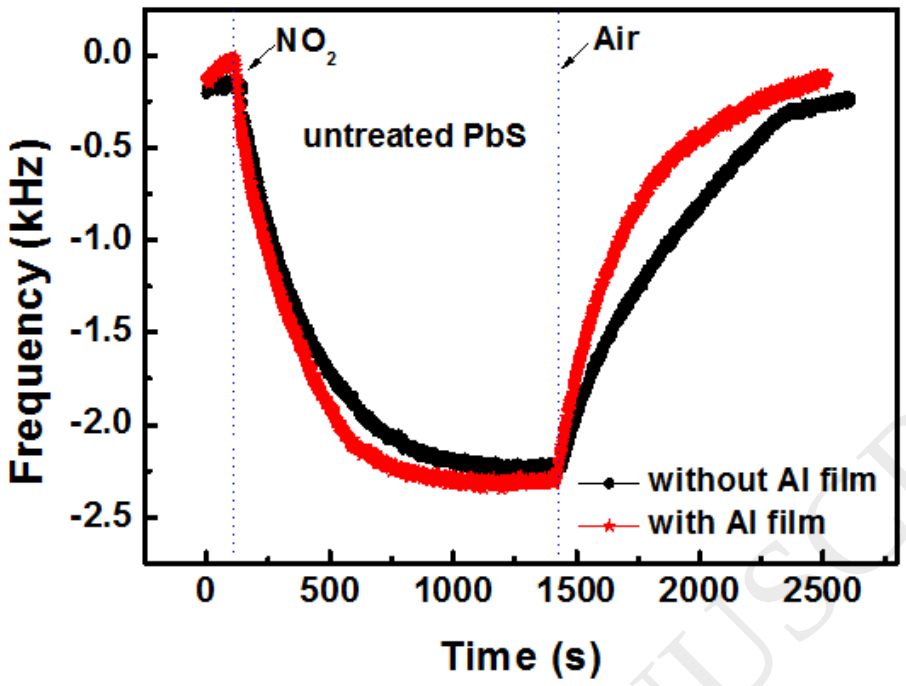

Fig. 8. (a) FTIR spectra of the untreated and $Pb(NO_3)_2$-treated PbS CQD films, (b) Schematic diagram of the ligand exchange process by $Pb(NO_3)_2$.

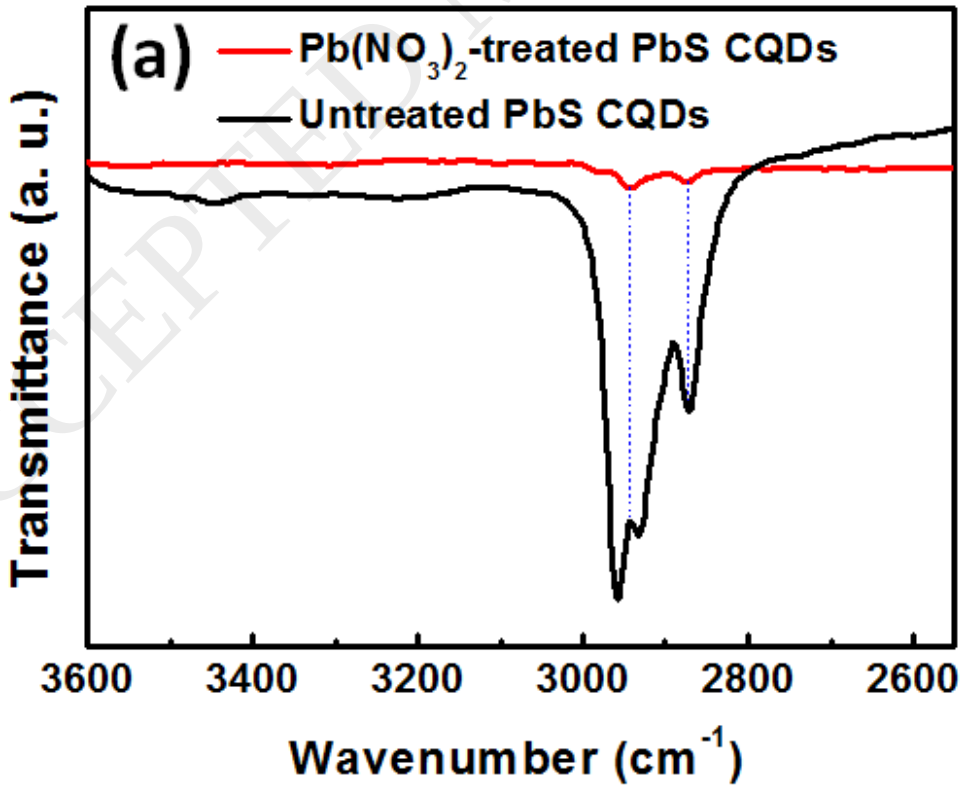

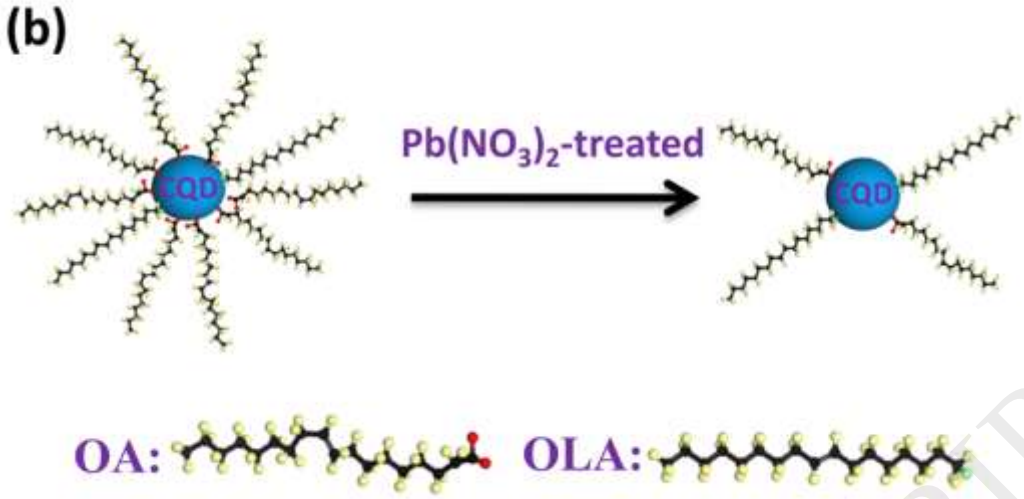

Fig. 9. SEM image of the untreated and $Pb(NO_3)_2$-treated PbS CQD films deposited on SAW devices.

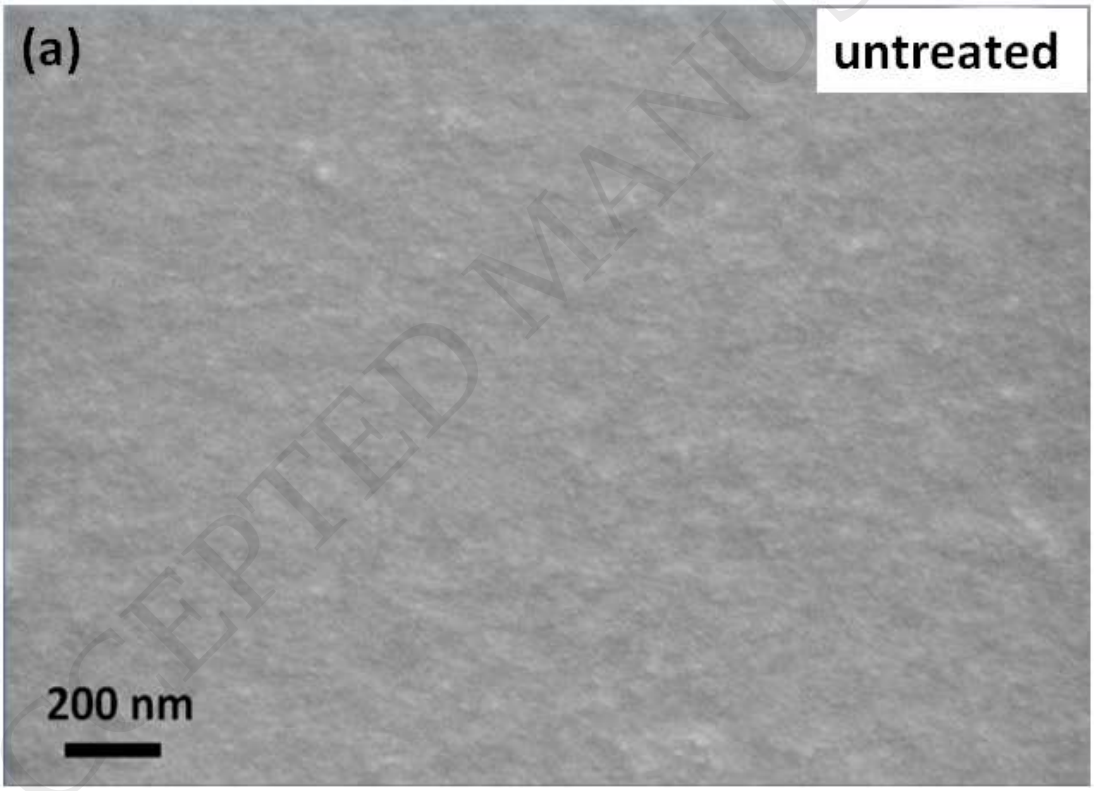

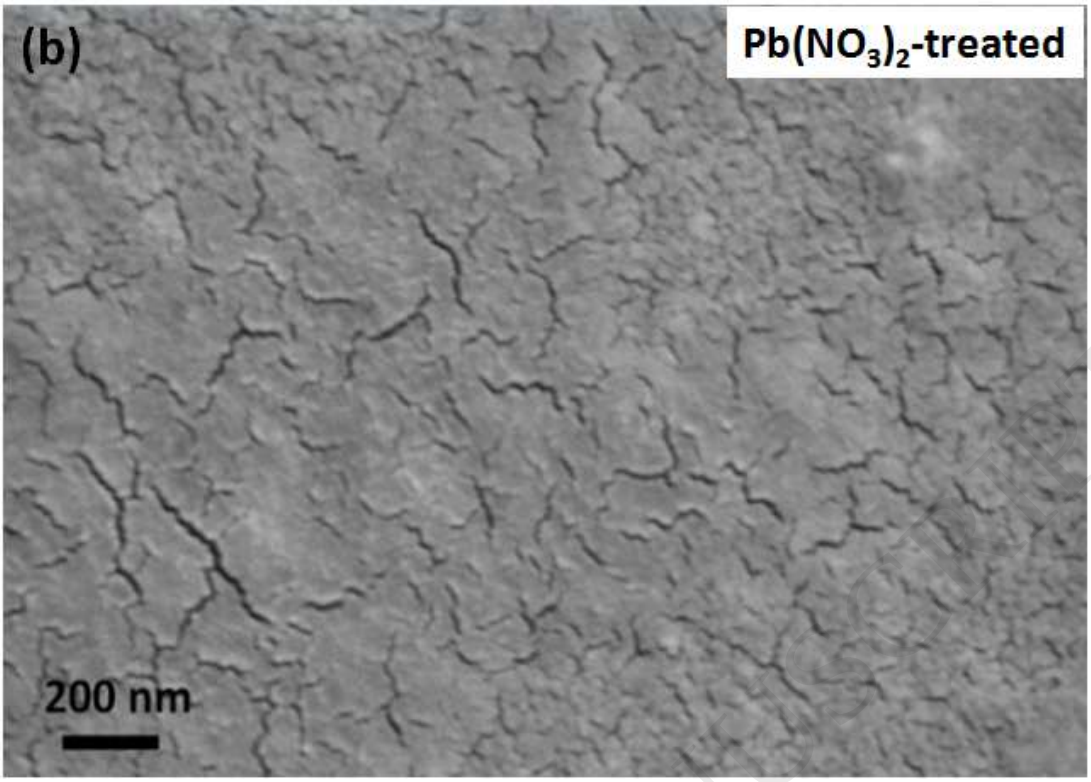

Fig. 10. Schematic diagrams on the gas sensing mechanism of the SAW gas sensors based on the untreated and $Pb(NO_3)_2$-treated PbS CQD films.

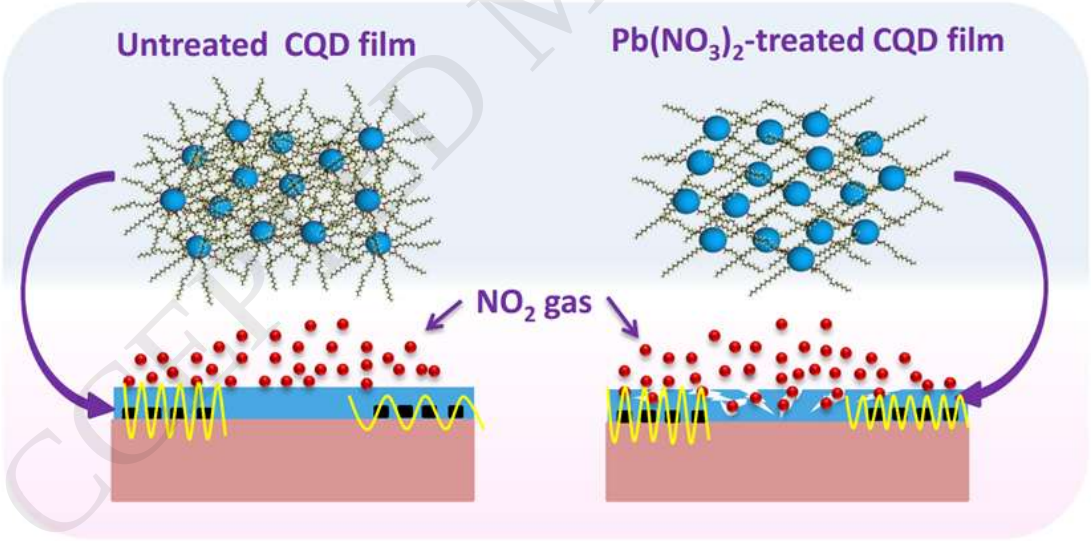

Fig. 11. (a) Transient response curves of the $Pb(NO_3)_2$-treated PbS CQD-based SAW sensor to 0.5-30 ppm NO_2 gas at room temperature, (b) Relationship of the sensor response and NO_2 concentration, (c) the stability and (d) the selectivity of the sensor.

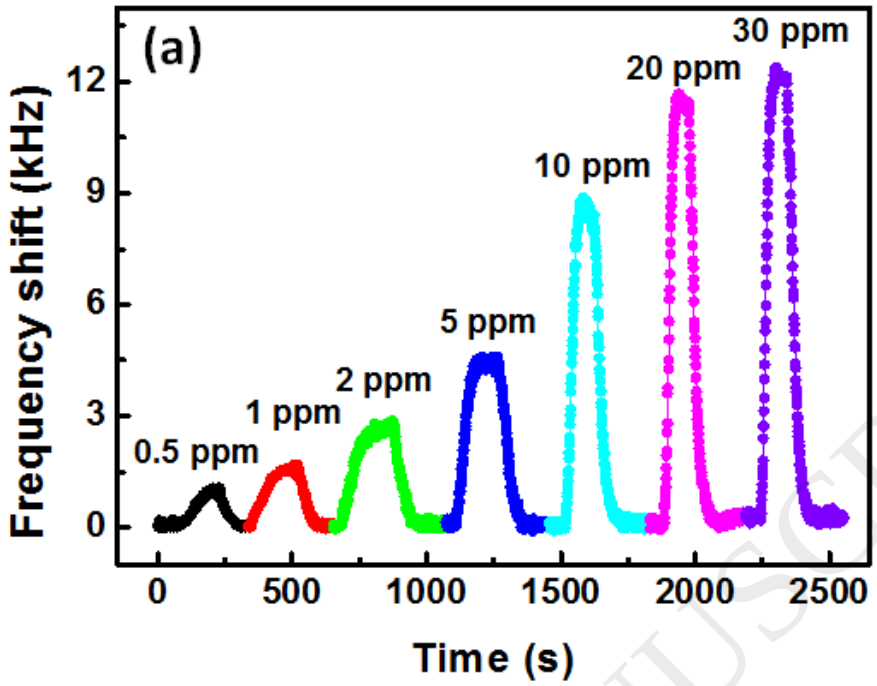

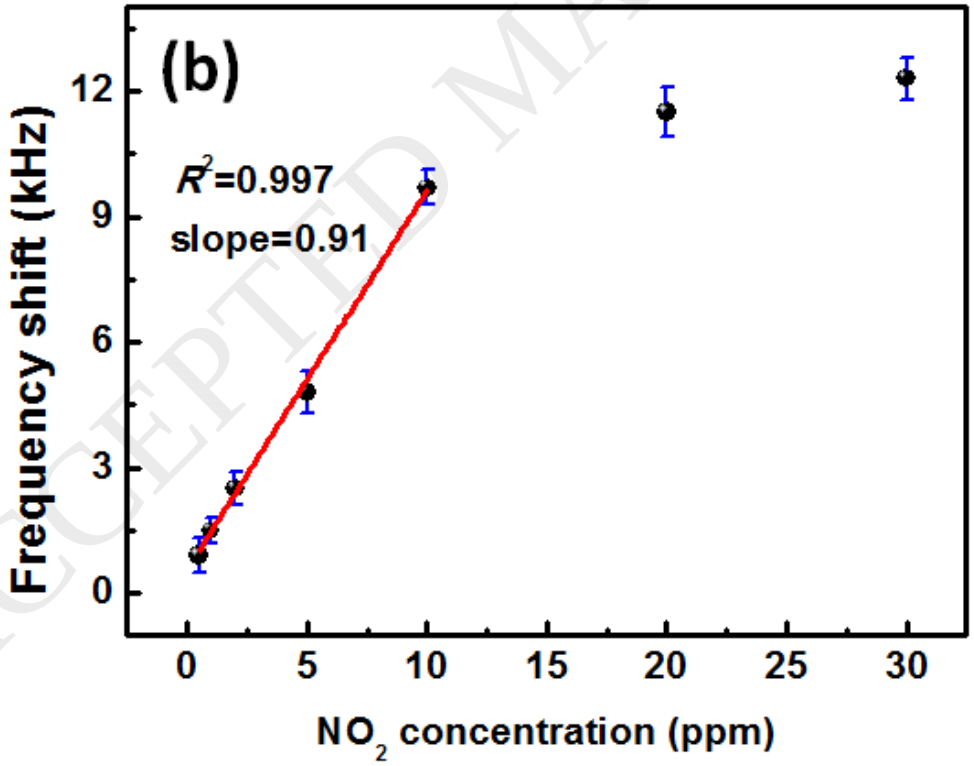

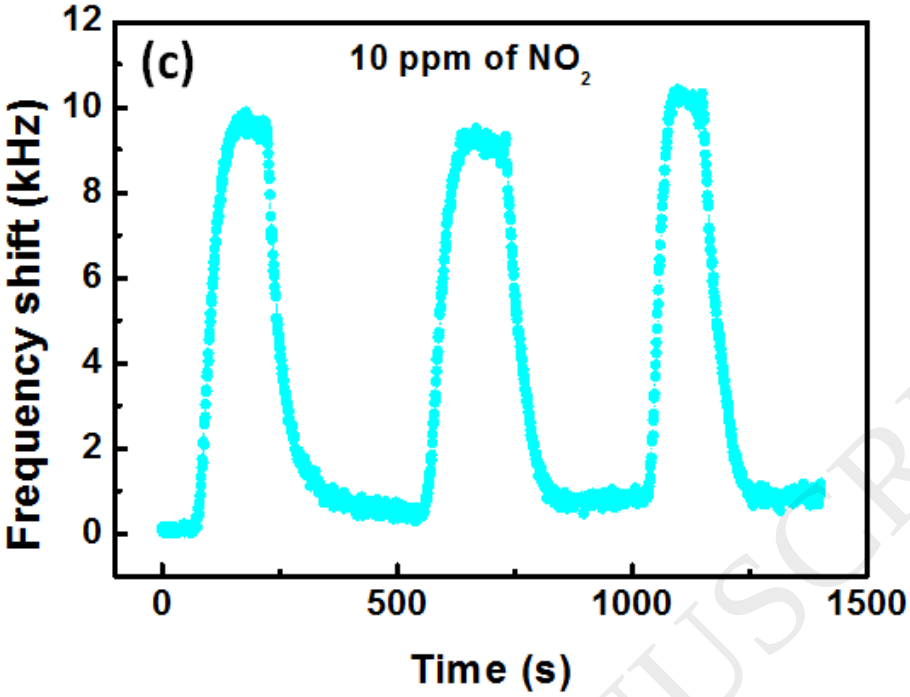

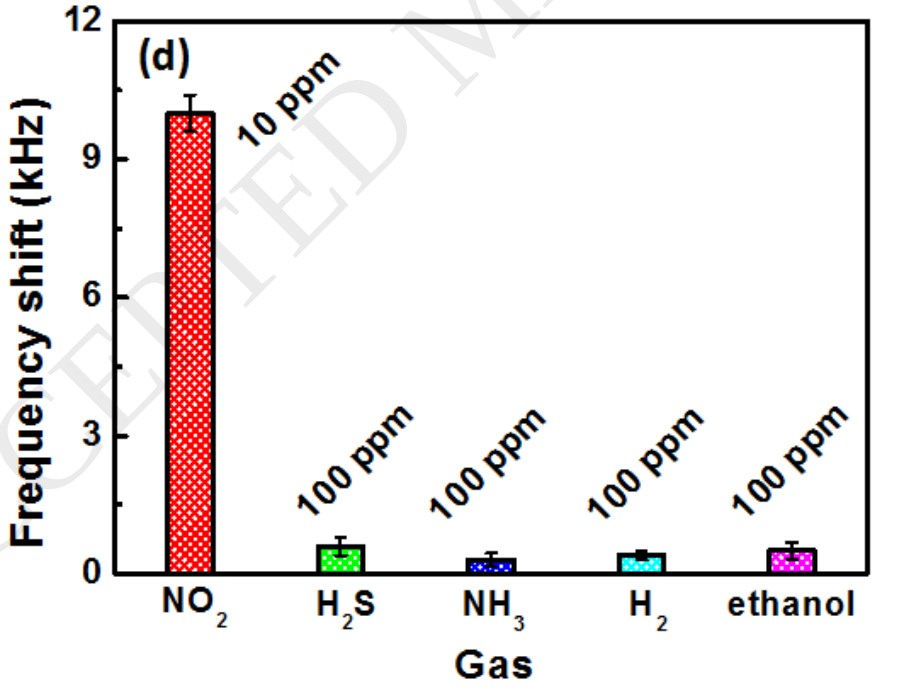

Table 1 NO_2-sensing properties of SAW gas sensors in this work and that reported in the literatures.

Materials	Method	Temperature	Concentration	Response	t_{res}/t_{rec}	Reference
PbS	Spin-coating	R.T.	10 ppm	9.8 KHz	45 s/58 s	This work
ZnO	RF magnetron sputtering	R.T.	0.4 ppm	6.0 KHz	hasn't been studied	[21]
PZT	Pulsed laser deposition	R.T.	80 ppm	1.1 KHz	hasn't been studied	[43]
CuPc/MWNTs	Spray-coating (150°C annealing)	R.T.	100 ppm	5.0 KHz	~300 s/1800 s	[44]
SnO_2	RF magnetron sputtering	R.T.	20 ppm	30 MHz	2 s/45 s	[40]
Graphene	Ink-jet printing	R.T.	3 ppm	0.08 KHz	~20 s/10 s	[45]
PPy/TiO_2	Dip-coating	R.T.	100 ppm	0.09 KHz	/	[46]
Polypyrrole	Drop-casting	R.T.	2.1 ppm	4.5 KHz	133 s/298 s	[47]
Polyaniline/In_2O_3	Drop-casting	R.T.	2.1 ppm	2.5 KHz	30 s/65 s	[48]
InO_x	DC sputtering	246°C	4.25 ppm	91 KHz	180 s/360 s	[49]
InO_x	DC sputtering	168°C	0.51 ppm	73.6 KHz	/	[50]